PROCEEDINGS OF SCIENCE

Dynamics and gravitational wave signatures of highly magnetized compact stars

Anson Ka Long Yip,[a,*] **Man Yin Leung,**[b] **Patrick Chi-Kit Cheong**[c,d] **and Tjonnie Guang Feng Li**[a,e,f]

[a] *Department of Physics, The Chinese University of Hong Kong, Shatin, N.T., Hong Kong*

[b] *Department of Physics, The Hong Kong University of Science and Technology, Clear Water Bay, Kowloon, Hong Kong*

[c] *Department of Physics & Astronomy, University of New Hampshire, 9 Library Way, Durham NH 03824, USA*

[d] *Department of Physics, University of California, Berkeley, Berkeley, CA 94720, USA*

[e] *Institute for Theoretical Physics, KU Leuven, Celestijnenlaan 200D, B-3001 Leuven, Belgium*

[f] *Department of Electrical Engineering (ESAT), KU Leuven, Kasteelpark Arenberg 10, B-3001 Leuven, Belgium*

E-mail: klyip@phy.cuhk.edu.hk, emilylmy1030@gmail.com, patrick.cheong@berkeley.edu, tjonnie.li@kuleuven.be

Strong magnetic fields make neutron stars potential sources of detectable electromagnetic and gravitational-wave signals. Hence, inferring these magnetic fields is critical to understand the emissions of neutron stars. However, the interior magnetic field configuration remains ambiguous due to the lack of direct observational evidence. Here, for the first time, we show that the internal magnetic field strength along with the composition of a neutron star can be directly constrained by detecting the gravitational waves from the phase-transition-induced collapse of a magnetized neutron star. In particular, we study the effects of magnetic fields and phase-transition-induced collapses on the dynamics, oscillation modes, and gravitational-wave signatures of compact stars through dynamical simulations. Hence, this work has demonstrated that much information inside neutron stars could be extracted by measuring the oscillation modes from the gravitational waves emitted by the stars.

38th International Cosmic Ray Conference (ICRC2023)
26 July - 3 August, 2023
Nagoya, Japan

*Speaker

PoS(ICRC2023)1518

1. Introduction

The strongest magnetic fields in the universe, up to 10^{14-15} G, are discovered on the surface of neutron stars. Some puzzling astronomical phenomena can be explained by these highly magnetized neutron stars, including soft gamma-ray repeaters and anomalous X-ray pulsars [1, 2]. Besides, the magnetic deformations on rotating neutron stars make them possible sources of continuous gravitational waves [3].

As the magnetic field governs the emissions of neutron stars, it is vital to interpret the magnetic field configurations of neutron stars. Nevertheless, even with the recently launched Neutron Star Interior Composition Explorer (NICER) [4], we can only interpret the surface magnetic field but not the interior magnetic field of neutron stars. Therefore, it is still challenging to determine the nature of the magnetic field inside neutron stars.

Detection of gravitational-wave signals from mergers of binary neutron stars provides a novel way of probing information inside the stars. Aside from binary mergers, excitation of oscillation modes in neutron stars could also produce detectable gravitational-wave signals. One possible scenario for exciting these oscillation modes is a phase-transition-induced collapse of a neutron star. When the rest-mass density in the neutron star core exceeds a certain threshold, a gravitational collapse is triggered by the phase transition from hadronic matter to deconfined quark matter in the core. This collapse results in a more compact 'hybrid star' composed of hadrons and deconfined quarks. Dynamical simulations were employed to study the dynamics and gravitational-wave signals of such a phase-transition-induced collapse [5, 6] . They demonstrated that fundamental modes of the resulting hybrid star can be excited and these modes give rise to detectable gravitational wave signals. However, the magnetic field was not considered in these studies.

In this proceeding, we present our recent works on simulating highly magnetized compact stars [7–9]. Specifically, we first discuss the pure magnetic effect (without considering any phase transition effect) on the oscillation modes of magnetized neutron stars with maximum magnetic field strength $\mathcal{B}_{\rm max} \sim 10^{15-17}$ G . Next, we describe the formation dynamics and the properties of a magnetized hybrid star formed from a phase-transition-induced collapse. Finally, we examine the gravitational-wave signatures from such a phase-transition-induced collapse and use these signatures to constrain the interior magnetic field configuration and the composition of the resulting hybrid stars.

2. Methodology

More details of the simulation set-ups can be found in Leung et al. [7] and Yip et al. [8, 9]. Here, we briefly highlight the important features of the set-ups.

2.1 Initial neutron star models

We construct equilibrium models of non-rotating magnetized neutron stars with purely toroidal magnetic fields by the open-sourced code `XNS` [10], which are the initial data for our simulation. We employ these equilibrium models with a polytropic equation of state $P = K\rho^\gamma$, where P denotes the pressure, ρ denotes the rest-mass density and we adopt a polytropic constant $K = 1.6 \times 10^5$ cm^5 g^{-1} s^{-2} (which is equivalent to 110 in the unit of $c = G = M_\odot = 1$) and a polytropic index $\gamma = 2$.

2.2 Evolution

The evolution of the neutron star models are studied by performing dynamical simulations with the code `Gmunu` [11]. We use two kinds of set-ups for the evolution for studying pure magnetic effects on neutron star oscillation modes (Section 2.2.1) and phase-transition-induced collapses of magnetized neutron stars (Section 2.2.2) respectively.

2.2.1 Pure magnetic effects on oscillation modes

We impose perturbations on the stellar models [12] and execute `Gmunu` once for each initial perturbation function. The models are evolved over a time span of 10 ms with the polytropic EoS $p = K\rho^\gamma$, under the same setting as in the computation of equilibrium models, namely, $\gamma = 2$ and $K = 1.6 \times 10^5$ cm^5 g^{-1} s^{-2} (which is equivalent to 110 in the unit of $c = G = M_\odot = 1$).

2.2.2 Phase-transition-induced collapses

Based on the framework introduced by Lin et al. [5], we assume that the phase transition happens instantaneously in the initial time slice and is triggered by changing the original polytropic equation to a "softer" equation of state for describing hybrid stars. The MIT bag model equation of state [13] for massless and non-interacting quarks is given by $P_\mathrm{q} = \frac{1}{3}(e - 4B)$, where P_q denotes the pressure of deconfined quarks, e denotes the total energy density and B denotes the bag constant. We apply the ideal gas equation of state to describe the evolution of normal hadronic matter $P_\mathrm{h} = (\gamma - 1)\rho\epsilon$, where P_h denotes the pressure of hadrons and γ is chosen to be 2.

A hybrid star formed after the phase-transition-induced collapse can be made up of two or three parts: (i) a hadronic phase for the region having a rest-mass density less than the lower threshold density $\rho < \rho_\mathrm{hm}$, (ii) a mixed phase of the deconfined quarks and hadrons for the region having a rest-mass density in between the lower threshold density and the upper threshold density $\rho_\mathrm{hm} < \rho < \rho_\mathrm{qm}$, and (iii) a region of pure quark matter phase with a rest-mass density beyond $\rho > \rho_\mathrm{qm}$ (the maximum density might or might not correspond to this phase in practice).

Following Abdikamalov et al. [6], the equation of state for hybrid stars can be expressed as follows:

$$P = \begin{cases} P_\mathrm{h} & \text{for } \rho < \rho_\mathrm{hm}, \\ \alpha_\mathrm{q} P_\mathrm{q} + (1 - \alpha_\mathrm{q}) P_\mathrm{h} & \text{for } \rho_\mathrm{hm} \le \rho \le \rho_\mathrm{qm}, \\ P_\mathrm{q} & \text{for } \rho_\mathrm{qm} < \rho, \end{cases} \tag{1}$$

where

$$\alpha_\mathrm{q} = 1 - \left(\frac{\rho_\mathrm{qm} - \rho}{\rho_\mathrm{qm} - \rho_\mathrm{hm}} \right)^\delta \tag{2}$$

quantifies the relative contribution of hadrons and deconfined quarks to the total pressure in the mixed phase. By using δ as the exponent, the pressure contribution due to deconfined quarks can be adjusted. We use 3 values of $\delta \in \{1, 2, 3\}$ to vary the pressure contribution due to deconfined quarks in the mixed phase. We take $\rho_\mathrm{hm} = 6.97 \times 10^{14}$ g cm^{-3}, $\rho_\mathrm{qm} = 24.3 \times 10^{14}$ g cm^{-3} and $B^{1/4} = 170$ MeV.

3. Results

3.1 Magnetic suppression on stellar oscillations

We plot the fundamental $l = 0$ quasi-radial mode frequency f_F (solid line) and the fundamental $l = 2$ quadrupolar mode frequency f_{2f} (dashed line) against the magnetic to binding energy ratio $\mathcal{H}/\mathcal{W}$ in left panel of Fig. 1. We observe an $\mathcal{H}/\mathcal{W}$ threshold for the magnetic field to start affecting the oscillation. For neutron stars with $\mathcal{H}/\mathcal{W} \lesssim 10^{-2}$, stellar oscillations are insensitive to magnetic effects. On the other hand, for neutron stars with $\mathcal{H}/\mathcal{W} \gtrsim 10^{-1}$ (corresponds to maximum magnetic field strength $\mathcal{B}_{\rm max} \sim 10^{17}$ G), stellar oscillations are significantly suppressed by stronger magnetic field.

The magnetic effects on neutron star oscillations discussed above could be understood by studying the compactness $M/R_{\rm circ}$ of the neutron star, where M is the gravitational mass and $R_{\rm circ}$ is the circumferential radius. As shown in Hartle and Friedman [14], the frequencies of the fundamental quasi-radial and quadrupole modes are related to the stellar compactness for non-magnetized neutron stars, and we suspect this correlation also holds for highly magnetized neutron stars. Thus, we plot in the right panel of Fig. 1 the compactness $M/R_{\rm circ}$ against the magnetic to binding energy ratio $\mathcal{H}/\mathcal{W}$. We find that $M/R_{\rm circ}$ remains nearly unchanged for $\mathcal{H}/\mathcal{W} \lesssim 10^{-2}$ but decreases dramatically for $\mathcal{H}/\mathcal{W} > 10^{-1}$, which agrees with the trends of $f(\mathcal{H}/\mathcal{W})$.

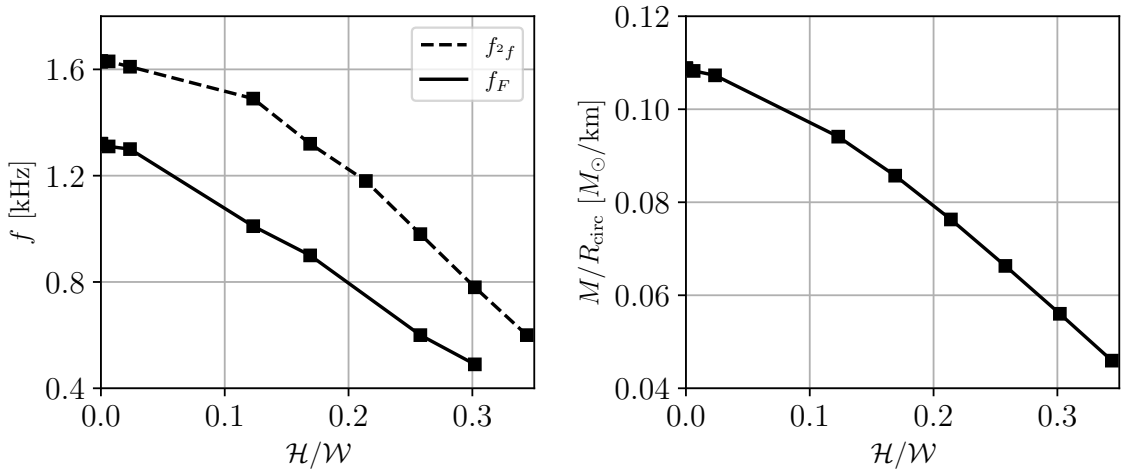

Figure 1: Left panel: Fundamental $l = 0$ quasi-radial mode frequency f_F (solid line) and fundamental $l = 2$ quadrupolar mode frequency f_{2f} (dashed line) against the magnetic to binding energy ratio $\mathcal{H}/\mathcal{W}$. Right panel: Compactness $M/R_{\rm circ}$ against the magnetic to binding energy ratio $\mathcal{H}/\mathcal{W}$.

3.2 Dynamics of phase-transition-induced collapses

We plot the time evolution of the maximum values of the rest-mass density $\rho_{\rm max}(t)$ (brown solid line) and the magnetic field strength $\mathcal{B}_{\rm max}(t)$ (dark cyan dash-dotted line) relative to their initial values $\rho_{\rm max}(0)$ and $\mathcal{B}_{\rm max}(0)$ in the left panel of Fig 2. The equilibrium values obtained at $t = 20$ ms are plotted with dashed lines. We observe similar damped oscillatory behaviors for both quantities and the star is relaxed into a new equilibrium configuration after the phase-transition-induced collapse.

We also illustrate the radial profiles of the rest-mass density $\rho(r)$ (top panel) and the magnetic field strength $\mathcal{B}(r)$ (bottom panel) at $t = 0$ ms (gray solid lines), 0.5 ms (red dash-dotted lines), 1.0 ms (orange dash-dotted lines), 5.0 ms (yellow dash-dotted lines), 10.0 ms (green dash-dotted lines), and 20.0 ms (blue dotted lines) in the right panel of Fig. 2. These profiles show that the phase-transition-induced collapse causes the resulting hybrid star eventually obtains a slightly higher central rest-mass density and maximum magnetic field strength. In addition, the magnetic field inside the star becomes more concentrated towards the core with a shift of the maximum magnetic field strength position $r_{\mathcal{B}}$ (dashed lines) to smaller values.

3.3 Properties of resulting magnetized hybrid stars

We plot in Fig. 3 central rest-mass density ρ_c (left panel) and baryonic mass fraction of the matter in the mixed phase M_{mp}/M_0 (right panel) against the maximum magnetic field strength $\mathcal{B}_{max}$. The data points of our resulting magnetized hybrid star models formed from phase-transition-induced collapses are arranged into 3 sequences with 3 values of $\delta \in \{1, 2, 3\}$, where δ is an exponent quantifying the pressure contribution due to quark matter in the mixed phase. We also plot the data points of our initial neutron star models before the phase transition collapses (red squares) as a comparison. For $\mathcal{B}_{max} \gtrsim 5 \times 10^{17}$ G, ρ_c drop significantly with $\mathcal{B}_{max}$, suppressing M_{mp}/M_0. When $\mathcal{B}_{max} \lesssim 3 \times 10^{17}$ G, ρ_c vary slightly with $\mathcal{B}_{max}$. Besides, ρ_c of the resulting magnetized hybrid star models vary with the $\mathcal{B}_{max}$ in the similar way as the initial neutron star models before the phase-transition-induced collapses. Therefore, this confirm that the magnetic effects on the initial neutron star equilibrium models still accurately describe their corresponding magnetized hybrid star models formed from phase-transition-induced collapses.

3.4 Gravitational-wave signatures

We find that the fundamental $l = 0$ quasi-radial F mode and the fundamental $l = 2$ quadrupolar ${}^2f$ mode are the 2 dominating peaks in the gravitational-wave spectrum. Hence, we plot the fundamental $l = 0$ quasi-radial mode frequency f_F and the fundamental $l = 2$ quadrupolar mode frequency f_{2f} against the maximum magnetic field strength $\mathcal{B}_{max}$ in the left panel of Fig. 4. Our data points are arranged into 3 sequences according to values of $\delta \in \{1, 2, 3\}$ used, where δ is an exponent describing the pressure contribution due to quark matter in the mixed phase. We also plot the data points of our initial neutron star models before the phase transition collapses (red squares) as a comparison. Both fundamental modes of the resulting hybrid stars decrease similarly to those initial neutron star models. Nonetheless, f_F in the resulting hybrid stars is smaller while f_{2f} is slightly larger when $\mathcal{B}_{max} \lesssim 5 \times 10^{17}$ G. These frequency differences depend on δ. f_F decreases with δ while f_{2f} increases with it. Hence, the magnetic suppression of stellar oscillations is still valid for the resulting magnetized hybrid stars and the mode frequency is also sensitive to δ.

To better illustrate the correlation between the fundamental mode frequencies and the properties of the resulting magnetized hybrid star, we plot a contour plot of the frequency ratio between the fundamental $l = 0$ quasi-radial mode and the fundamental $l = 2$ quadrupolar mode f_{2f}/f_F against the maximum magnetic field strength $\mathcal{B}_{max}$ (horizontal axis) and the baryonic mass fraction of matter in the mixed phase M_{mp}/M_0 (vertical axis) in Fig. 4. We constructed this plot by the cubic radial basis function interpolation of the data points of our models. A colored dot with a black edge labels each data point. The dash-dotted lines denote the contour lines for particular values

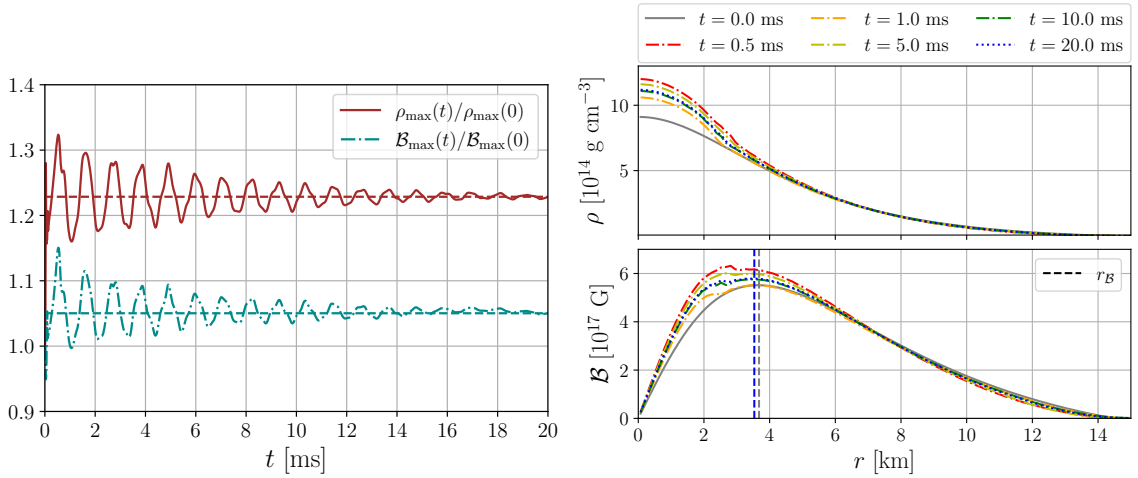

Figure 2: Left panel: Time evolution of the maximum values of the rest-mass density $\rho_{\max}(t)$ (brown solid line) and the magnetic field strength $\mathcal{B}_{\max}(t)$ (dark cyan dash-dotted line) relative to their initial values $\rho_{\max}(0)$ and $\mathcal{B}_{\max}(0)$ for the simulation with an initial maximum magnetic field strength $\mathcal{B}_{\max} = 5.52 \times 10^{17}$ G and the exponent $\delta = 3$. Dashed lines are the equilibrium values of the two quantities obtained at $t = 20$ ms. Right panel:The radial profile of the rest-mass density $\rho(r)$ (top panel) and the magnetic field strength $\mathcal{B}(r)$ (bottom panel) in the equatorial plane for the same simulation at $t = 0$ ms (gray solid lines), 0.5 ms (red dash-dotted lines), 1.0 ms (orange dash-dotted lines), 5.0 ms (yellow dash-dotted lines), 10.0 ms (green dash-dotted lines), and 20.0 ms (blue dotted lines).

of f_{2f}/f_F. For a fixed value of f_{2f}/f_F, there are localized regions in the $\mathcal{B}_{\max}$ - $M_{\rm mp}/M_0$ plane. Therefore, the measurement of f_{2f}/f_F constrains the values of $\mathcal{B}_{\max}$ and $M_{\rm mp}/M_0$.

4. Conclusions

In this proceeding, we have presented several works on dynamically simulating highly magnetized compact stars. In particular, we first found that the oscillation mode frequency of a neutron star is suppressed when the maximum magnetic field strength $\mathcal{B}_{\max} \sim 10^{17}$ G. Next, we showed that the magnetic effects on initial equilibrium models still accurately describe the hybrid stars formed by phase-transition-induced collapse. Finally, we illustrated that the fundamental modes of the stars can be used to constrain $\mathcal{B}_{\max}$ together with the baryonic mass fraction of matter in the mixed phase $M_{\rm mp}/M_0$ of the stars. Consequently, taking $\mathcal{B}_{\max}$ and $M_{\rm mp}/M_0$ as examples, this work has demonstrated that much information inside neutron stars could be extracted through measuring the oscillation modes of the stars.

References

[1] C. Kouveliotou, S. Dieters, T. Strohmayer, J. van Paradijs, G. J. Fishman, C. A. Meegan, K. Hurley, J. Kommers, I. Smith, D. Frail, and T. Murakami. An X-ray pulsar with a superstrong magnetic field in the soft γ-ray repeater SGR1806 - 20. *Nature*, 393(6682):235–237, May 1998.

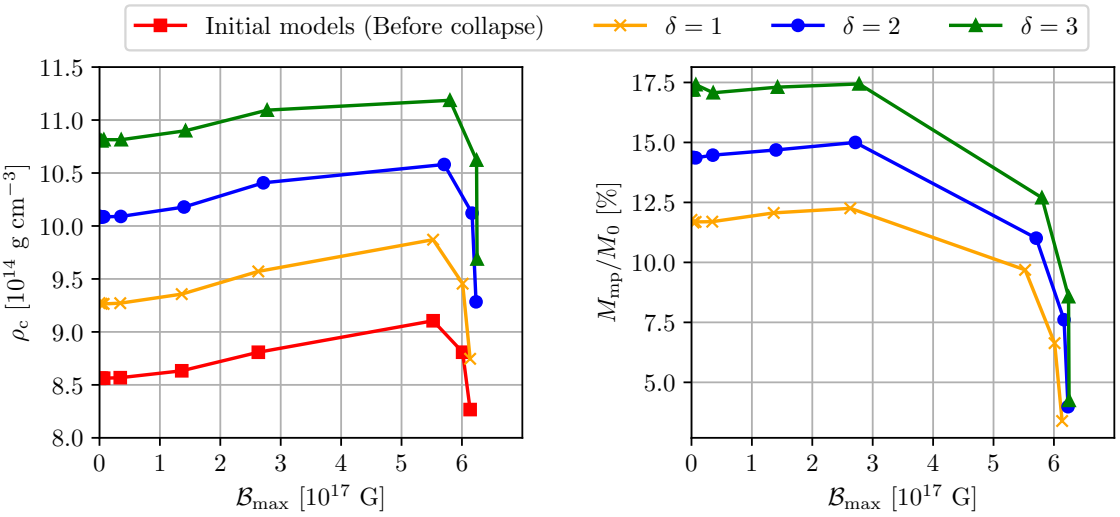

Figure 3: Left panel: Central rest-mass density ρ_c against the maximum magnetic field strength $\mathcal{B}_{max}$. Right panel: Baryonic mass fraction of the matter in the mixed phase M_{mp}/M_0 against the maximum magnetic field strength $\mathcal{B}_{max}$.

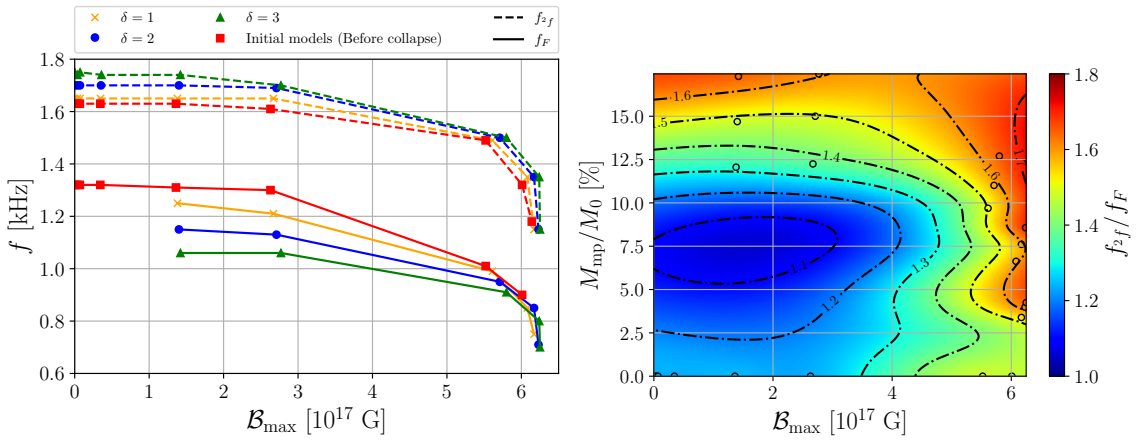

Figure 4: Left panel: Fundamental $l = 0$ quasi-radial mode frequency f_F and fundamental $l = 2$ quadrupolar mode frequency f_{2f} against the maximum magnetic field strength $\mathcal{B}_{max}$. Right panel: Contour plot of the frequency ratio between the fundamental $l = 0$ quasi-radial mode and the fundamental $l = 2$ quadrupolar mode f_{2f}/f_F against the maximum magnetic field strength $\mathcal{B}_{max}$ (horizontal axis) and the baryonic mass fraction of matter in the mixed phase M_{mp}/M_0 (vertical axis).

[2] S. Mereghetti, D. Cremonesi, M. Feroci, and M. Tavani. BeppoSAX observations of SGR 1806-20 SAX observations of SGR 1806-20. *Astron. Astrophys.*, 361:240–244, September 2000.

[3] S. Bonazzola and E. Gourgoulhon. Gravitational waves from pulsars: emission by the magnetic-field-induced distortion. *Astron. Astrophys.*, 312:675–690, August 1996.

[4] A. V. Bilous, A. L. Watts, A. K. Harding, T. E. Riley, Z. Arzoumanian, S. Bogdanov, K. C.

Gendreau, P. S. Ray, S. Guillot, W. C. G. Ho, and D. Chakrabarty. A NICER View of PSR J0030+0451: Evidence for a Global-scale Multipolar Magnetic Field. *Astrophys. J. Lett.*, 887(1):L23, December 2019.

[5] L. M. Lin, K. S. Cheng, M. C. Chu, and W. M. Suen. Gravitational Waves from Phase-Transition-Induced Collapse of Neutron Stars. *Astrophys. J.*, 639(1):382–396, March 2006.

[6] Ernazar B. Abdikamalov, Harald Dimmelmeier, Luciano Rezzolla, and John C. Miller. Relativistic simulations of the phase-transition-induced collapse of neutron stars. *Mon. Not. R. Astron. Soc.*, 392(1):52–76, January 2009.

[7] Man Yin Leung, Anson Ka Long Yip, Patrick Chi-Kit Cheong, and Tjonnie Guang Feng Li. Oscillations of highly magnetized non-rotating neutron stars. *Communications Physics*, 5(1):334, December 2022.

[8] Anson Ka Long Yip, Patrick Chi-Kit Cheong, and Tjonnie Guang Feng Li. General-relativistic simulations of the formation of a magnetized hybrid star. *arXiv e-prints*, page arXiv:2303.16820, March 2023.

[9] Anson Ka Long Yip, Patrick Chi-Kit Cheong, and Tjonnie Guang Feng Li. Gravitational wave signatures from the phase-transition-induced collapse of a magnetized neutron star. *arXiv e-prints*, page arXiv:2305.15181, May 2023.

[10] N. Bucciantini and L. Del Zanna. General relativistic magnetohydrodynamics in axisymmetric dynamical spacetimes: the X-ECHO code. *Astron. Astrophys.*, 528:A101, April 2011.

[11] Patrick Chi-Kit Cheong, Alan Tsz-Lok Lam, Harry Ho-Yin Ng, and Tjonnie Guang Feng Li. Gmunu: paralleled, grid-adaptive, general-relativistic magnetohydrodynamics in curvilinear geometries in dynamical space-times. *Mon. Not. R. Astron. Soc.*, 508(2):2279–2301, December 2021.

[12] Harald Dimmelmeier, Nikolaos Stergioulas, and José A. Font. Non-linear axisymmetric pulsations of rotating relativistic stars in the conformal flatness approximation. *Mon. Not. Roy. Astron. Soc.*, 368(4):1609–1630, June 2006.

[13] Kenneth Johnson et al. The mit bag model. *Acta Phys. Pol. B*, 6(12):8, 1975.

[14] James B. Hartle and John L. Friedman. Slowly Rotating Relativistic Stars. VIII. Frequencies of the Quasi-Radial Modes of an N = 3/2 Polytrope. *Astrophys. J.*, 196:653–660, March 1975.